Communications in Physics, Vol. 34, No. 4 (2024), pp. 425-436

DOI: https://doi.org/10.15625/0868-3166/20945

Developing computational and experimental models of heat transfer through multi-layered textile structures

Nguyen Ngoc Son, Nguyen Dinh Phuong, Do Xuan Doanh, Tong Minh Hoa, Nguyen Anh Tuan † and Nguyen Manh Thang ‡

Academy of Military Science and Technology, 17 Hoang Sam, Nghia Do, Cau Giay, Hanoi, Vietnam

E-mail: †tuanvn.vn@gmail.com; ‡thangnm@jmst.info

Received 16 June 2024; Accepted for publication 25 October 2024; Published 8 November 2024

Abstract. Object signature management is a critical and urgent task that helps conceal and restrict the detection of contemporary optoelectronic systems. The design of thermal camouflage textiles and material solutions constitutes a significant scientific area, however, publications in this area are restricted because of military competitiveness and technological secrecy. Research on thermal camouflage materials has garnered interest both domestically and internationally for various purposes, especially in military applications. Multi-layered textile structures offer several advantages, including a simple structure, the ability to combine multiple materials with different properties, and wide applicability. The article presents a simple model for computing and simulating heat transfer through multi-layer textiles, along with tests to assess the heat suppression effect and heat radiation energy of some samples of multi-layer textiles made of domestic materials. The initial computational and experimental results provide an important foundation for further research and application of multi-layered textile structures.

Keywords: thermal signature management; multi-layered textile structures; thermal camouflage; heat transfer; background.

Classification numbers: 42.79.Dj; 44.10.+i; 81.05.Lg.

1. Introduction

With the strong development of sensor technology, objects can now be easily identify utilizing medium- and long-wavelength infrared emission indicators thanks to advanced optoelectronic systems with greater sensitivity and resolution [1–3]. This has a direct impact and presents several challenges in the signature management of vital objects to restrict detection by enemy optoelectronic systems, thereby contributing to safety and force preservation [4, 5]. One effective solution for managing object signatures is to apply camouflage measures to reduce or eliminate the object's signature, particularly its thermal signature [6–8].

©2024 Vietnam Academy of Science and Technology

An object's thermal signature is generated by the thermal contrast between the object and its background. This contrast is influenced by the material's characteristics, surface structure, and environmental factors [6–8]. Thermal imaging devices capture an object's thermal signature through the thermal radiation it emits, which is dependent on the emission coefficient, radiation wavelength, the object's temperature, and environmental conditions. According to Stefan-Boltzmann's law, the radiative power of an object is a function of its fourth power temperature and emission coefficient (ε) [5–8]. Therefore, thermal camouflage solutions focus on two main approaches: adjusting the object's temperature, modifying its emission coefficient, or combining both strategies. As a result, various thermal camouflage materials have been developed. These include paints, thin films that cover an object's surface directly, cover plates, nets, canvas, and other materials designed to conceal the object. Additionally, self-adaptive smart camouflage systems have been developed, which continuously adjust an object's temperature and emission coefficient to blend seamlessly with its surroundings [7, 8]. However, the thermal signature of large objects, such as structures and mobile vehicles, greatly depends on the temperature difference (ΔT) between the target and the background. This ΔT is a crucial parameter for developing thermal camouflage solutions focused on temperature adjustment [9]. Smaller ΔT values result in low target detection likelihood and shorter detection distances, while larger ΔT values lead to higher detection capabilities and longer detection distances. To reduce ΔT , a common method is to use multi-layer thermal camouflage textiles. This approach involves layering multiple materials to lower the temperature of the object's surface through heat exchange effects [9–15]. Multi-layer thermal camouflage textiles have been widely employed for the thermal camouflage of mobile vehicles across various countries and represent a promising and highly feasible research direction in our country [15].

The article primarily covers the introduction of the general model for calculating heat exchange through the multi-layer textiles, temperature measurement experiments, simulation calculations using MATLAB, and radiation energy measurements for several multi-layer thermal camouflage textile samples made from available materials. The simulation and experimental results are presented and discussed in Sec. 3. The conclusion and directions for further research are presented in Sec. 4.

2. Theoretical background, numerical model, simulations and experiment

This section introduces the fundamental theory of thermal imaging systems and a simple model for heat transfer through multi-layered textile structures (MTS). Using existing materials and simulations, the study optimizes the layering of these materials and evaluates the effectiveness of thermal camouflage for the selected MTS.

2.1. Theoretical background

The thermal imaging system (TIS) captures images of the object according to the diagram shown in Fig. 1 [16]. An object's thermal signature describes the spatial distribution of its irradiance, and it is captured by the thermal imaging system. The object's irradiance is a complex number due to the interaction of the radiation qualities of the object and the background (emission coefficient, reflection coefficient, and temperature), as well as scattering on the atmospheric transmission path before going to the thermal detector [17].

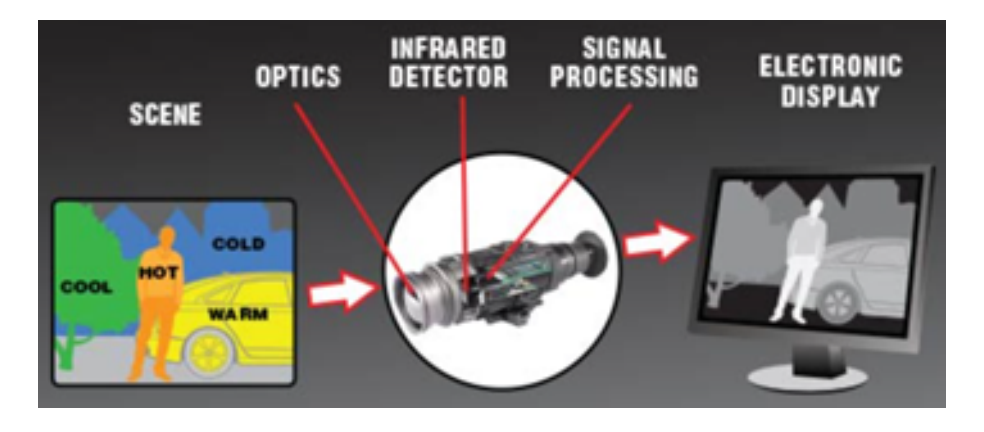


Fig. 1. The basic components of a thermal imaging system (TIS).

Thermal imaging systems employ irradiance differences to generate thermal images. To simplify the description of the object's thermal signature, it is typical to use the temperature difference between the target and the background ΔT according to the formula [17]:

$$\Delta T = T_{TG} - T_{BG},$$

$$T_{TG} \propto \int_{\lambda_1}^{\lambda_2} \oint_{A_{TG}} \left[\varepsilon_{TG}(x, y, \lambda) \cdot L_{TG}(x, y, T(x, y)) + \rho_{TG} \cdot M_{ES, TG}(x, y, \lambda) \right] dx dy d\lambda,$$

$$T_{BG} \propto \int_{\lambda_1}^{\lambda_2} \oint_{A_{RG}} \left[\varepsilon_B(x, y, \lambda) \cdot L_{BG}(x, y, T(x, y)) + \rho_{BG} \cdot M_{ES, BG}(x, y, \lambda) \right] dx dy d\lambda,$$

$$(1)$$

where the symbols "TG" and "BG" denote the target and the background, respectively. T_{TG} and T_{BG} represent the temperatures of the target and the background, ε represents the emissivity, ρ represents the reflectance, L represents the blackbody radiance (W/(m².sr. μ m)), T represents the local temperature (K), and M represents the irradiation from external radiation sources (W/m²). The above value is integrated over the area A_{TG} or A_{BG} (m²), within the spectral range from λ_1 to λ_2 (μ m).

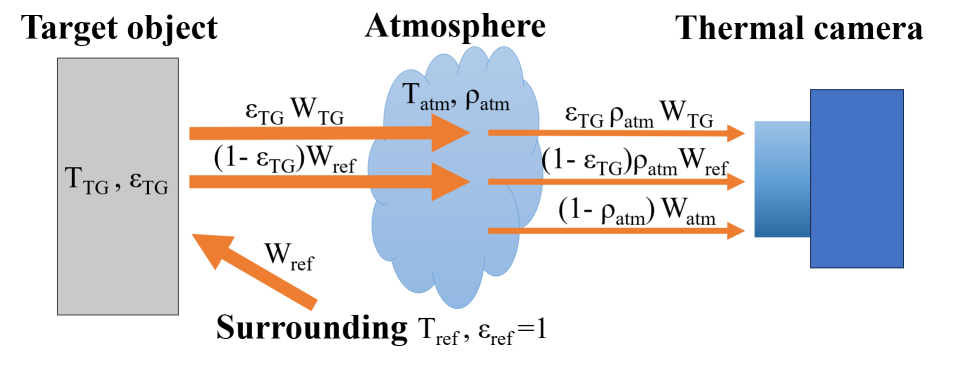


Fig. 2. Diagram of temperature measurement by thermal camera [18].

Heat energy can be transferred in three ways: conduction, convection and radiation. The thermal radiation detected by the TIS consists of three sources: (1) emission from the target W_{TG} , (2) emission from the surroundings reflected on the target W_{ref} , and (3) emission from the atmosphere W_{atm} , as illustrated in Fig. 2. The total thermal radiation captured by the TIS (denoted as W_{TIS} (W/m²)) is quantified by the following formula [18–20]:

$$W_{TIS} = \varepsilon_{TG} \cdot \rho_{atm} \cdot W_{TG} + (1 - \varepsilon_{TG}) \cdot \rho_{atm} \cdot W_{ref} + (1 - \rho_{atm}) \cdot W_{atm}, \tag{2}$$

where ρ_{atm} represents the atmospheric transmittance. It is assumed that the reflected radiation from the surroundings has a uniform temperature T_{ref} with an emissivity coefficient ε_{ref} equal to one. The radiation emitted by the object, and reflected radiation is partially absorbed by the atmosphere along the transmission path. Additionally, atmospheric radiation is emitted from the atmosphere between the object and the TIS at the background temperature T_{atm} , with an emissivity coefficient of "1- ρ_{atm} ". The value of ρ_{atm} depends on T_{atm} , humidity and the distance between the object and the TIS. To calculate in-band radiance, an integration function similar to formula (1) can be derived by incorporating the components from formula (2) [21].

2.2. Numerical model of heat transfer through MTS

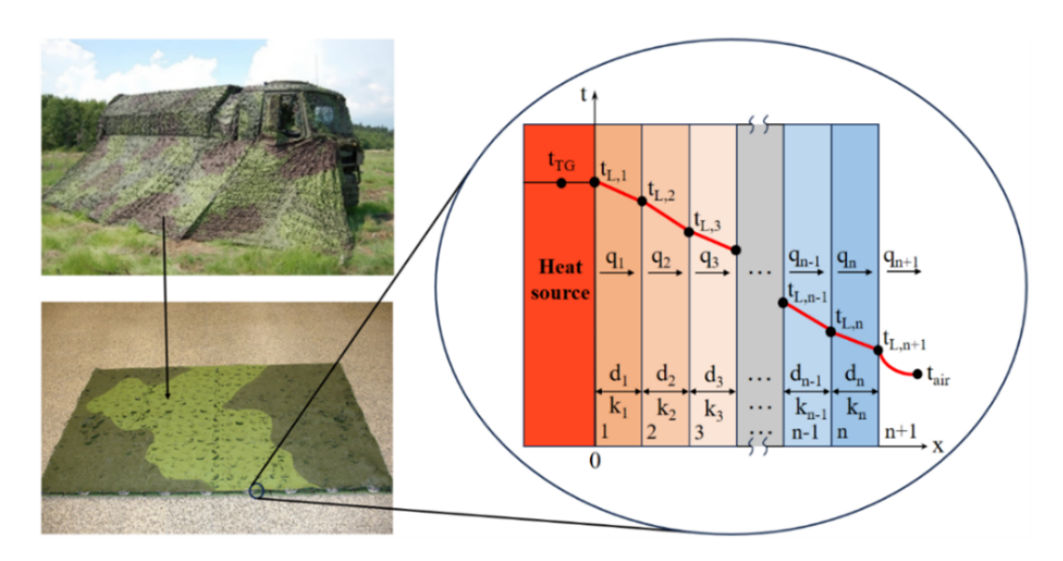


Fig. 3. Diagram of heat transfer through n layer MTS.

A multi-layer textile is made up of overlapping single layers of material. The thermal camouflage textile is applied directly to the object being concealed. The thermal imaging device will then get the temperature from the object as it passes through the textile via heat transfer mechanisms. As a result, the thermal camouflage textile is designed and manufactured to keep the coating surface temperature within the desired range. Assume that the multi-layer textile consists of n distinct layers of flat material with isotropic thermal properties, as illustrated in Fig. 3. For simplicity, the analysis excludes the effect of contact thermal resistance between these layers [22].

Consider a method of static heat transfer through n layers of flat material, with each layer having a surface temperature $t_{L,I}$ (°C), thickness d_i (mm) and heat transfer coefficient k_i (i=1,2,...,n)

 $(W/(m\cdot K))$, respectively. Assuming steady state heat transfer $(q_i=q_{i+1} \text{ for } i=1,2,\ldots,n+1)$, and that the thermophysical properties of the material are constant, the temperature in the coating changes linearly [23, 24]. Thus, the heat transfer diagram in Figure 3 includes: the temperature t_{TG} and the ambient temperature t_{air} are constant, and the continuous heat transfer from $t_{L,1}$ to $t_{L,n+1}$. Thus, the heat transfer process from t_{TG} to t_{air} will include: heat conduction from t_{TG} to $t_{L,n+1}$, and both heat convection and heat emission from $t_{L,n+1}$ to t_{air} . The heat flow density q_1 transmitted from the heat source through the first material layer by conduction (denoted as q_{cond} (W/m^2)), and through layers 2, 3, ..., n with corresponding heat flow densities $q_2,...,q_n$ can be calculated as follows [23]:

$$q_{cond} = q_1 = (t_{L,1} - t_{L,2}) \cdot \frac{k_1}{d_1} = \dots = q_n = (t_{L,n} - t_{L,n+1}) \cdot \frac{k_n}{d_n} = \frac{t_{TG} - t_{L,n+1}}{\sum_{i=1}^n \frac{d_i}{k_i}}.$$
 (3)

The heat flow density q_{n+1} from the n-th surface to the ambient air layer, including thermal convection in the air and thermal emission from the surface, is calculated as follows:

$$q_{n+1} = q_{conv} + q_{rad} = q_{cond}$$

$$= \alpha \cdot (t_{I,n+1} - t_{oir}) + \sigma \cdot \varepsilon \cdot (t_{I,n+1}^4 - t_{oir}^4), \tag{4}$$

where α , σ and ε are the exothermic coefficients, the Stefan-Boltzmann constant and the surface emission coefficients of the n-th material layer respectively. Assume the material system consists of 3 (n=3) layers, and set $p_i=k_i/d_i$ (i=1, 2, ..., n). Since the heat flow density from the heat source and through the material layers is constant, $q_1=q_2=q_3$, the following formulas can be applied:

$$p_1 \cdot (t_{TG} - t_{L,2}) = p_2 \cdot (t_{L,2} - t_{L,3}),$$

$$p_1 \cdot t_{TG} - (p_1 + p_2) \cdot t_{L,2} + p_2 \cdot t_{L,3} = 0,$$
(5)

$$p_2 \cdot (t_{L,2} - t_{L,3}) = p_3 \cdot (t_{L,3} - t_{L,4}),$$

$$p_2 \cdot t_{L,2} - (p_2 + p_3) \cdot t_{L,3} + p_3 \cdot t_{L,4} = 0.$$
(6)

We also have $q_3 = q_4$, so:

$$p_{3} \cdot (t_{L,3} - t_{L,4}) = \alpha \cdot (t_{L,4} - t_{air}) + \sigma \cdot \varepsilon \cdot (t_{L,4}^{4} - t_{air}^{4})$$

$$p_{3} \cdot t_{L,3} - (p_{3} + \alpha) \cdot t_{L,4} = -\alpha \cdot t_{air} + q_{rad}.$$
(7)

Thus, for a number of layers n > 3, the following equations apply:

$$-(p_{1}+p_{2}) \cdot t_{L,2} + p_{2} \cdot t_{L,3} + 0 \cdot t_{L,4} + \dots + 0 \cdot t_{L,n+1} = -p_{1} \cdot t_{TG},$$

$$p_{2} \cdot t_{L,2} - (p_{2}+p_{3}) \cdot t_{L,3} + p_{2} \cdot t_{L,4} + 0 \cdot t_{L,5} + \dots + 0 \cdot t_{L,n+1} = 0,$$

$$0 \cdot t_{L,2} + p_{3} \cdot t_{L,3} - (p_{3}+p_{4}) \cdot t_{L,4} + p_{4} \cdot t_{L,5} + \dots + 0 \cdot t_{L,n+1} = 0,$$

$$\vdots$$

$$0 \cdot t_{L,2} + \dots + p_{n-1} \cdot t_{L,n-1} - (p_{n-1}+p_{n}) \cdot t_{L,n} + p_{n} \cdot t_{L,n+1} = 0,$$

$$0 \cdot t_{L,2} + \dots + 0 \cdot t_{L,n-1} + p_{n} \cdot t_{L,n} - (\alpha+p_{n}) \cdot t_{L,n+1} = -\alpha \cdot t_{air} + q_{rad}.$$

$$(8)$$

If we arrange the matrices \mathbf{A} , \mathbf{x} and \mathbf{B} in the following form:

$$\mathbf{A} = \begin{pmatrix} -(p_{1} + p_{2}), p_{2}, 0, \cdots, 0 \\ p_{2}, -(p_{2} + p_{3}), p_{3}, 0, \cdots, 0 \\ 0, p_{3}, -(p_{3} + p_{4}), p_{4}, 0, \cdots, 0 \\ \vdots \\ 0, \cdots, p_{n-1}, -(p_{n-1} + p_{n}), p_{n} \\ 0, \cdots, 0, 0, p_{n}, -(\alpha + p_{n}) \end{pmatrix}, \quad \mathbf{x} = \begin{pmatrix} t_{L,2} \\ t_{L,3} \\ t_{L,4} \\ \vdots \\ t_{L,n} \\ t_{L,n+1} \end{pmatrix}, \quad \mathbf{B} = \begin{pmatrix} -p_{1} \cdot t_{TG} \\ 0 \\ 0 \\ \vdots \\ 0 \\ -\alpha \cdot t_{air} + q_{rad} \end{pmatrix}$$
(9)

The system of equations (8) will be written in a simple form as follows:

$$\mathbf{A} \cdot \mathbf{x} = \mathbf{B} \tag{10}$$

Given the known values of the material layers and the deterministic values of α , t_{TG} , t_{air} and q_{rad} , A and B are deterministic, so we calculate the value of x as the surface temperature values of the material layers according to the following formula, where A^{-1} is the inverse matrix of A:

$$\mathbf{x} = \mathbf{A}^{-1} \cdot \mathbf{B}.\tag{11}$$

To measure the textile surface temperature, use the HT 9815 Contact Thermometer, to measure q_{rad} emitted from the object, use the heating source RaSou-12 and the SR-5000N Spectroradiometer [26], with a measured spectral range from 2.5 μ m to 14 μ m.

2.3. Simulations

Based on the multi-layer textile model and the formulas (3), (4), (9) and (11) presented in subsection 2.2, develop a calculation program on MATLAB software. The basic parameters of the material layers, measured at the Center for High Technology Research and Development, Vietnam Academy of Science and Technology, are shown in the following Table 1:

Table 1. Materials used to prepare the multi-layer textile sample.

Code	Group	Thickness	Quantity	Thermal
			(g/cm2)	Conductivity
				coefficient
		(mm)		$(W/(m \cdot K))$
I1	I-Inside	0.12	0.013	0.543
I2	(Metallic	0.16	0.021	0.083
I3	coating)	0.10	0.008	0.259
M1		5	0.048	0.103
M2	M-Middle (3D textile)	8	0.058	0.102
M3		15	0.079	0.141
O1		0.49	0.038	0.650
O2	O-Outside	0.43	0.024	0.383
O3	(Camouflage print textile)	0.21	0.021	0.641
O4		0.11	0.008	0.281

Randomly select materials from each of the three sets of materials (I, M, O) and combine them in the sequence specified in Table 2:

Table 2. Multi-layer assembly of materials from existing materials.

Number of	Sort order	Number of multi-layer	
material layers		material sample combinations	
3	I-M-O	3x3x4=36	
4	I-M-I-O	3x3x3x4=108	

Run the software program in each case according to the amount of material layers (3 or 4), and can modify the number of layers to benefit the power of the calculation speed. However, the authors only concentrate on two cases of 3 layers and 4 layers of material as represented within the scope of the article due to the limited number of material samples and to minimize the experimental volume; in the case of more material layers, the calculation and experimental steps are similar. Note that, in (4), the temperature factors $t_{L,n+1}$ have a great influence on the values q_{rad} and q_{n+1} , so for each case of 3 layers and 4 layers of material, we need to find the layered combination with the smallest surface temperature in the outermost material layer $t_{L,n+1}$ to test the sample.

2.4. Experiments

According to the simulation results, the material combination that produces the lowest tem-

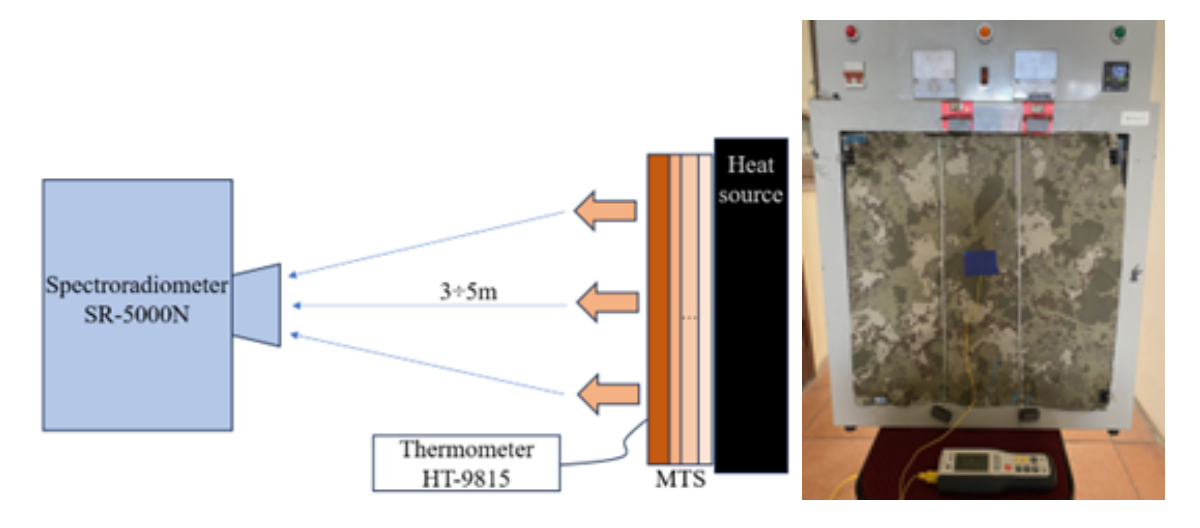


Fig. 4. Schematic diagram of thermal suppression measurement.

perature at the outermost surface for each case of 3 and 4 layers is identified. Multi-layer textile samples shall be produced experimentally using the aforementioned combination. Place the multi-layer textiles on the heating plate in turn according to the test diagram as shown in Fig. 4, and

measure the surface temperature with the HT-9815 Contact Thermometer and the radiation energy with the SR-5000N Spectroradiometer. The SR-5000N's optical objective is set at a field of view of 2 mrad, 5 m from the heating plate [26].

The heating plate is set to a temperature that is significantly higher than of the medium. In this article, the heating plate is adjusted at 50° C and 80° C, with an ambient temperature of 30° C. To calculate the thermal camouflage effect, the concept of thermal suppression efficiency T_{S} (%) provided by MTS is used, according to the following formula [9]:

$$T_S(\%) = \frac{T_{TG} - T_{MTS}}{T_{TG} - T_{RG}} \times 100, \tag{12}$$

where $T_{\rm TG}$, $T_{\rm BG}$, $T_{\rm MTS}$ are respectively the temperature of the heating plate, the ambient temperature and the outermost surface temperature of the MTS.

To calculate the heat radiation energy degrading effect of the textile, at this time the formula (12) becomes the heat radiation energy degradation effect T_{RD} (%) of the MTS according to the following formula (13) [27]:

$$T_{RD}(\%) = \left(1 - \frac{E_{MTS,80} - E_{MTS,50}}{E_{TG,80} - E_{TG,50}}\right) \times 100,$$
 (13)

where $E_{\rm MTS,80}$ and $E_{\rm MTS,50}$ represent the radiation from the textile when cladding it to the heating plate (camouflaged target) at 80°C and 50°C, respectively. $E_{\rm TG,80}$ and $E_{\rm TG,50}$ represent the radiation from the heating plate (non-camouflaged target) at 80°C and 50°C, respectively. These values will be measured in units of (W/(cm²·sr)) using the SR-5000N Spectroradiometer [26].

3. Results and discussion

3.1. Model calculation results

From the materials in Table 1 and formulas (3) and (4), we can see that for the minimum surface temperature t_{n+1} of the n-th layer, we are given a 3-layer material combination of I2M3O2 and a 4-layer material combination I2M3I2O2. Applying the formula (9) and (11) with the values set as t_{TG} =50°C and t_{TG} =80°C, t_{air} =30°C, assuming α =13.6 (W/(m²·°C)) and t_{TG} =30°C, taken from the measurement results in the following section), we can calculate the surface temperature of the material layers as follows:

```
3 layers: t_{TG}=50^{\circ}\text{C}, q_{rad}=84 \text{ W/m}^2: t_{L,2}=49.7^{\circ}\text{C}, t_{L,3}=34.5^{\circ}\text{C}, t_{L,4}=34.3^{\circ}\text{C}. t_{TG}=80^{\circ}\text{C}, q_{rad}=95 \text{ W/m}^2: t_{L,2}=79.4^{\circ}\text{C}, t_{L,3}=46.3^{\circ}\text{C}, t_{L,4}=45.9^{\circ}\text{C}. 4 layers: t_{TG}=50^{\circ}\text{C}, q_{rad}=86 \text{ W/m}^2: t_{L,2}=49.7^{\circ}\text{C}, t_{L,3}=34.6^{\circ}\text{C}, t_{L,4}=34.3^{\circ}\text{C}, t_{L,5}=34.1^{\circ}\text{C}. t_{TG}=80^{\circ}\text{C}, q_{rad}=88 \text{ W/m}^2: t_{L,2}=79.4^{\circ}\text{C}, t_{L,3}=46.9^{\circ}\text{C}, t_{L,4}=46.3^{\circ}\text{C}, t_{L,5}=46^{\circ}\text{C}.
```

3.2. Experimental result

The surface temperature of the outermost layer of the 3-layer (I2M3O2) and 4-layer (I2M3I2O2) textiles when applying them to the heating plate surface at 50°C and 80°C respectively measured by HT-9815 with an ambient temperature of 30°C are shown in the following Fig. 5:

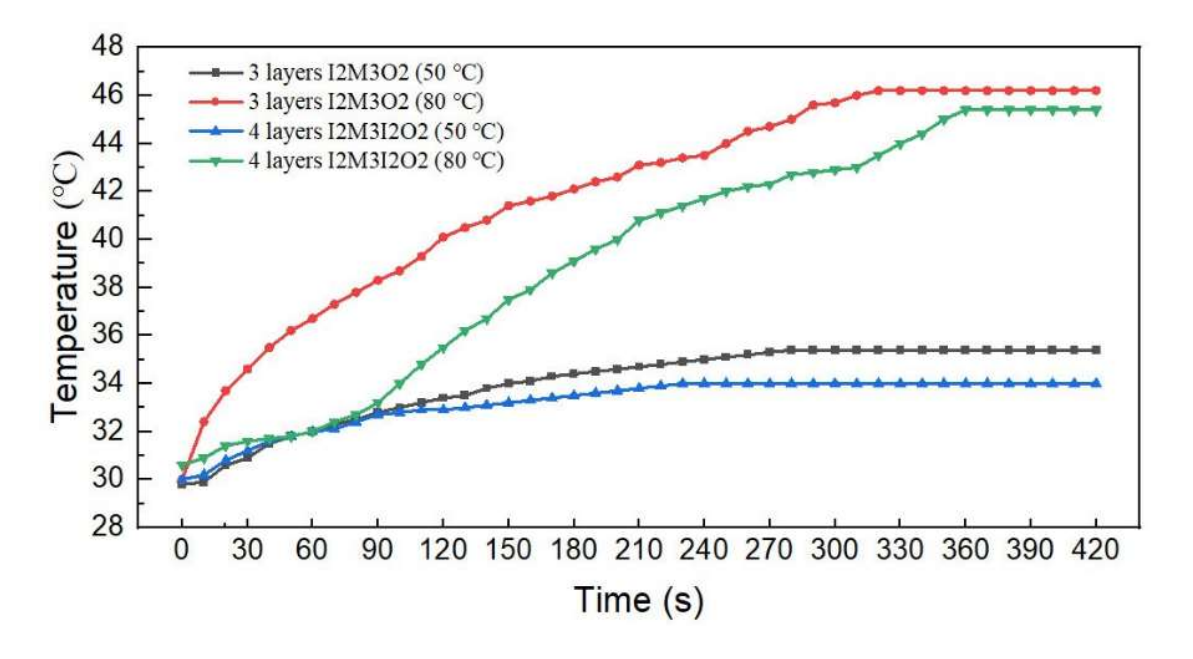


Fig. 5. The surface temperature of the textiles when applied to the heat source.

With these results, it is found that, when the heating plate temperature is set at 80°C, the textile surface temperature increases rapidly and begins to stabilize after about 6 minutes with surface temperatures of 46.2°C (3-layer) and 45.4°C (4-layer), respectively. Where the heating plate temperature is set at 50°C, the textile surface temperature increases more slowly and gradually stabilizes after about 4 minutes with surface temperatures of 35.4°C (3-layer) and 34°C (4-layer), respectively. The surface temperatures measured by the contact thermometer are close to the calculated results in subsection 3.1, but the discrepancy between the simulation and actual measurements may be due to contact thermal resistance.

In addition, at 60 seconds, the temperature of the 3-layer I2M2O2 (50°C) and 4-layer I2M2I2O2 at both 50°C and 80°C has the same value and then increases. This may be explained because, in the material structure, the first two layers, including I2 and M2, are the same, therefore when initially exposed to the heating plate, the outermost layer temperature is the same. However, with the 3-layer I2M2O2 (80°C), because the heating plate temperature is high and the number of layers is minimal, the temperature transfers to the outermost layer extremely quickly, leading to a greater surface temperature than other textiles.

At both heating plate temperatures, the 4-layer textile had a lower surface temperature than the 3-layer textile. Using the formula (12), we can compute the thermal suppression efficiency of the textiles, as indicated in the Table 3.

The findings of monitoring the surface temperature of the textile using a contact thermometer show that the 4-layer textile has a greater thermal suppression efficiency than the 3-layer textile. This means that the more layers a material has, the more heat suppression it has. Using this method, we can totally design a structured textile with the appropriate number of layers of materials to achieve excellent thermal suppression efficiency.

Multi-layer textile	The heating plate at	The heating plate at	
	temperature 50°C	temperature 80°C	
3 layers - I2M3O2	73%	67.6%	
4 layers - I2M3I2O2	80%	69.2%	

Table 3. The textile's thermal suppression efficiency at the temperature values.

Continue measuring the radiance of the heat source with and without the MTS using the SR-5000N Spectroradiometer [26], the results are shown in Fig. 6. The results in Fig. 6 show

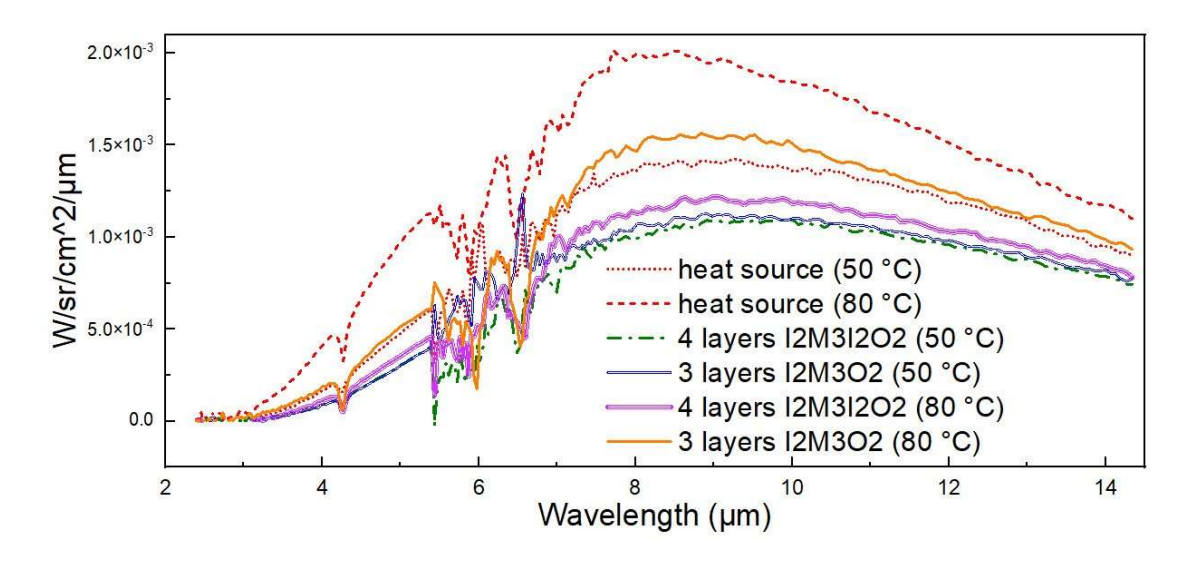


Fig. 6. Spectral radiance of the heat source with and without the MTS.

that, at heating plate temperatures of 50°C and 80°C, the 4-layer textile has a lower peak of the irradiation power spectrum density per unit mass angle than the 3-layer textile, indicating that the 4-layer textile effectively shields the heat radiation. It can be seen that in the 8 μ m to 12 μ m range, there is the highest irradiation power density compared to other spectral regions. Besides, multi-layer textiles are remarkably effective in reducing the irradiation power spectrum density. In the range of 2.5 μ m to 7 μ m, it can be seen that the irradiation power density is strongly reduced due to two major reasons: the heating plate at 50°C to 80°C is mainly emitted in the range of 8 μ m to 14 μ m and less emitted in the range of 3 μ m to 5 μ m because this is a low temperature range, similar to the temperature of a person when actively moving and the surfaces when absorbing solar irradiation.

The results demonstrate that the 4-layer textile more efficiently reduces irradiance compared to the 3-layer textile. Across the entire measured spectrum of the SR-5000N, the 4-layer textile reduced irradiance by up to 92%.

Table 4. The textile's radiation reduction efficiency.

Multi-layer textile	Spectrum 3 μm÷5 μm	Spectrum 8 μm÷14 μm	Whole range 2.5 μm÷14 μm
3 layers - I2M3O2	83%	64%	68%
4 layers - I2M3I2O2	91%	82%	92%

4. Conclusion

This article developed a simple model to calculate the temperature distribution of material layers in multi-layer thermal camouflage textiles, performed simulation calculations for design optimization, and produced trial samples to test the textile's heat suppression effect and irradiation reduction efficiency.

Based on the results from 10 available material samples and the model's calculations, two textile structures were selected: a 3-layer structure with the order I2M3O2 and a 4-layer structure with the order I2M3I2O2. Testing revealed that, at an ambient temperature of 30°C, the 4-layer textile (I2M3I2O2) outperforms the 3-layer textile in terms of thermal suppression efficiency. Specifically, the 4-layer textile achieved efficiencies of 80% and 69.2% at heating plate temperatures of 50°C and 80°C, respectively. Additionally, the SR-5000N Spectroradiometer measurements showed that the 4-layer textile had greater irradiation reduction efficiency compared to the 3-layer textile, with reductions of 91% in the 3 μ m to 5 μ m range, 82% in the 8 μ m to 14 μ m range and 92% in the 2.5 μ m to 14 μ m range.

Based on the obtained results, the authors will further refine the calculation model and incorporate a material library to optimize the layering design. This will aid in the development of an MTS that effectively shields the heat and reduces target radiation, making it suitable for practical applications.

Acknowledgments

The authors would like to thank Institute of Technical Physics, AMST, and Center for High Technology Research and Development, VAST, for their support.

References

- [1] A. Rogalski, Infrared detectors: an overview, Infrared Phys. Tech. 43 (2002) 187.
- [2] G.C. Holst, Common Sense Approach to Thermal Imaging, JCD and SPIE Pub., 2000, pp. 265–290.
- [3] J. Barela, K. Firmanty and M. Kastek, *Measurement and Analysis of the Parameters of Modern Long-Range Thermal Imaging Cameras*, Sensors **21** (2021) 5700.
- [4] F.B. Olsen, Methods for evaluating thermal camouflage, A FFI Report No. RTO-MP-SCI-145, (2005) 1.
- [5] C. Plesa, D. Turcanu and V. Bodoc, *The use of infrared radiation for thermal signatures determination of ground targets*, Rom. J. Phys. **51** (2006) 63.
- [6] JV.R. Rao, Introduction to Camouflage and Deception, Ministry of Defence, New Delhi-110 011 (1999) 21.
- [7] M. C. Hall, *Thermal signature management*, Master thesis, North Carolina State University, USA (2017).
- [8] K. Andersson, *On the military utility of spectral design in signature management: a system approach*, Doctoral dissertation, Finnish National Defence University, Finland (2018).
- [9] O. Dev, S. Dayal, A. Dubey and S.M. Abbas, *Multi-layered textile structure for thermal signature suppression of ground-based targets*, Infrared Phys. Tech. **105** (2020) 103175.

- [10] Hexels, Thermal camouflage sheet, US Patent US7244684 B2 (2007).
- [11] M. Hellwig and J. Weber, Thermal Camouflage Tarpaulin, US Patent US7148161 B2 (2006).
- [12] P.R. Cox, J. C. Edwards, J. S. Loyd and L. Watkins, *Infrared Camouflage Covering*, US Patent US6127007 (2000).
- [13] G.D. Culler, Infra-red reflective coverings, US Patent US5750242 (1998).
- [14] V. Rubeziene, I. Padleckiene, S. Varnaite-Zuravliova and J. Baltusnikaite-Guzaitiene, Reduction of thermal signature using textiles with conductive additives, Mater. Sci. (Medziagotyra) 19 (2013) 409.
- [15] N. N. Son, N. M. Thang, V. D. Hieu and N. A. Tuan, Advances in manufacturing multi-layer materials for thermal camouflage applications, J. Mil. Sci. Technol. 97 (2024) 3.
- [16] User Manual ThermoCAMTM P65, FLIR System, (2006) 185.
- [17] D. Peric, B. Livada, M. Peric and S. Vujic, Thermal Imager Range: Predictions, Expectations and Reality, Sensors 19 (2019) 3313.
- [18] K. Tomita and M.Y.L. Chew, A Review of Infrared Thermography for Delamination Detection on Infrastructures and Buildings, Sensors 22 (2022) 423.
- [19] T. Williams, Thermal imaging cameras: Characteristics and performance, Boca Raton: CRC Press (2009).
- [20] P. A. Jacobs, Thermal infrared characterization of ground targets and backgrounds, SPIE (2006).
- [21] V. D. Hieu, N. H. Hai and N. N. Son, Experiment to evaluate the effectiveness of thermal reflective coating applied to constructions, Journal of Science and Technique 7 (2024) 152.
- [22] H. R. Han, Y. Park, C. Yun, and C. H. Park, *Heat transfer characteristics of aluminum sputtered fabrics*, Journal of Engineered Fibers and Fabrics, **13** (2018) 37.
- [23] Y. Cengel and A. Ghajar, Heat and Mass Transfer: Fundamentals and Applications, Mc. Hill Edu. (2015) 144.
- [24] A. Das, A. Ramasamy and K.P. Kumar, Study of heat transfer through multilayer clothing assemblies: a theoretical prediction, AUTEX Res. J. 11 (2011) 54.
- [25] N.N. Son, N.D. Phuong, T.T. Bao, T.M. Hoa, N.T. Lam, D.X. Doanh et al, A high-accuracy measurement method of surface emissivity using a spectroradiometer SR-5000N, Proc. of 8th CASEAN, 28-30 Aug., Vinh (2023) 674.
- [26] SpectroRadiometer Model SR-5000N Operation and Maintenance Manual, CI Systems, (2014) 2.
- [27] G. Gillberg, A. Grop and M. Nysten, Technical specification MLCN, FMV (2013) 8.